University of Sistan and Baluchestan

Challenges in Nano and Micro Scale Science and Technology

Online ISSN: 2821 - 000X

Heat Transfer Dynamics in Hydrophobic Microchannels: A Study of Non-Newtonian Fluids under Magnetic Influence

Fardis Azizi[1] | Keivan Fallah[2]✉ | Hossein Zolfaghari Azizi[3] | Soroush Madah[4]

Department of Mechanical Engineering, Sari Branch, Islamic Azad University, Sari, Iran.
Department of Mechanical Engineering, Sari Branch, Islamic Azad University, Sari, Iran. Email: Keyvan.fallah@gmail.com; keyvan.fallah@iau.ac.ir
Department of Mechanical Engineering, Sari Branch, Islamic Azad University, Sari, Iran.
Department of Mechanical Engineering, Sari Branch, Islamic Azad University, Sari, Iran.

Article Info

Article type:
Research Article

Keywords:
Lattice Boltzmann Method,
Non-Newtonian fluid,
Hydrophobic surfaces,
Microchannel,
Magnetic field

ABSTRACT

This study explores the heat transfer (HT) characteristics of non-Newtonian fluids in hydrophobic microchannels influenced by magnetic fields (MFs). Using the Lattice Boltzmann Method (LBM), a detailed two-dimensional microscale model is developed to analyze the combined effects of flow slippage, viscous dissipation, and temperature jump phenomena. The power-law model is employed to represent the non-Newtonian fluid behavior accurately. The results demonstrate that increasing the slip length significantly enhances convective HT by modifying boundary layer dynamics. However, this enhancement is mitigated by the opposing effects of temperature jump and viscous dissipation. The introduction of a magnetic field further alters the flow dynamics, with the Lorentz force optimizing velocity profiles and substantially boosting HT efficiency. The results show that the presence of magnetic field with Ha=20 enhances heat transfer 3.3% and 4.2% at B=0 and B=0.06 respectively for non-Newtonian fluid flow with n=0.9. These findings underline the intricate interplay between magnetic field intensity, fluid rheology, and surface properties, offering valuable guidance for designing advanced thermal management systems in microchannel applications.

F	external force	ω_α	Weight corresponding to the lattice direction α
dt	Time step	ρ	Fluid density
$f_\alpha(x,t)$	Distribution function	u	Velocity vector
τ_w	Shear rate	c_s	Speed of sound in the lattice
$f_\alpha^{eq}(x,t)$:	Equilibrium distribution function	p	pressure
$g_\alpha(x,t)$	temperature distribution function	ν	Kinematic viscosity
τ	Relaxation time	$T(x,t)$	Macroscopic temperature
τ_s	thermal relaxation time	$\dot{\gamma}$	Shear rate
μ	Viscosity	K	Consistency coefficient
D_h	Hydraulic diameter	N	flow behavior index
C_p	Heat capacity	**MF**	Magnetic field
K	Thermal conductivity	**GPU**	Graphic Processor unit
Re	Reynolds number	**PEC**	thermal performance
h	Heat transfer coefficient	**subscript**	
Br	Brinkmann number	α	lattice velocity direction.
Pr	Prandtl	**App**	apparent
Nu	Nusselt number	**S**	sound
HTC	Heat transfer coefficient	**F**	fluid
DF	Distribution function	**W**	wall
C_f	Friction coefficient	**Reff**	refference
θ_j	Nondimensional temperature	**B**	bulk
B	Nondimensional slip coefficient	**ave**	average
Γ	Heat capacity ratio	**superscript**	
ζ^*	Temperature jump coefficient	**eq**	equilibrium

How to Cite this paper: Azizi F., Fallah K., Zolfaghari Azizi H., Madah S. Heat Transfer Dynamics in Hydrophobic Microchannels: A Study of Non-Newtonian Fluids under Magnetic Influence. *Challenges in Nano and Micro Scale Science and Technology*. 2024; 12(1): 1-11. DOI: 10.22111/cnmst.2025.50927.1257

© Azizi F., Fallah K., Zolfaghari Azizi H., Madah S. Publisher: University of Sistan and Baluchestan.
DOI: 10.22111/cnmst.2025.50927.1257

INTRODUCTION

The examination of heat transfer (HT) in microscale channels has garnered considerable attention due to its critical applications in various engineering domains, including micro pumps, mixing chambers, and cooling of electronic boards. Numerous studies have reviewed this field, highlighting its significance and potential for innovation [1-5]. One approach to enhancing HT in such systems is the addition of nanoparticles to a base fluid, forming a nanofluid. Nanofluids exhibit improved HT characteristics due to factors such as enhanced thermal conductivity, Brownian motion, increased surface area, higher specific heat capacity, boundary layer reduction, and electrophoresis. However, challenges such as instability, increased viscosity, erosion-corrosion effects, and health concerns associated with nanofluids limit their applicability in specific scenarios. Comprehensive reviews, such as those by Eneren *et al*. [6] and Kumar *et al*. [7], provide insights into the role of nanofluids in HT enhancement within microchannels.

Nanofluids can transform a Newtonian fluid into a non-Newtonian one due to the interactions and behaviors of the suspended particles. While Newtonian fluids exhibit constant viscosity independent of shear rate, the addition of nanoparticles introduces complexities such as Brownian motion, particle collisions, and fluid-particle interactions, resulting in non-linear rheological behavior. At higher nanoparticle concentrations, these interactions intensify, leading to shear-thinning or shear-thickening properties. Furthermore, nanoparticle aggregation alters the microstructure of the fluid, adding to the complexity. Thus, the rheological properties of nanofluids depend on particle size, shape, concentration, and interactions with the base fluid [8-10].

Given the challenges of experimental studies at the microscale, numerical simulations have become essential tools in this field [11, 12]. Recent advancements have explored the application of hydrophobic and superhydrophobic surfaces as well as magnetic fields (MFs) to enhance HT rates and the thermal performance (PEC) of microchannels. A magnetic field enhances heat transfer in magnetohydrodynamic (MHD) flow by generating a Lorentz force that modifies fluid motion, thinning hydrodynamic and thermal boundary layers to improve convective heat transfer, suppressing turbulence to stabilize flow, inducing secondary vortices for better mixing, and increasing effective thermal conductivity through forced alignment of conductive particles or Joule heating, particularly in electrically conducting fluids like liquid metals or plasmas, making it useful in applications such as nuclear cooling, electronic cooling, and aerospace thermal management. For example, Rahbarshahlan *et al*. [13] demonstrated that hydrophobic patterns reduce average velocity by 12% in the developed region. Yao *et al*. [14] reported improved thermal performance with hydrophobic surfaces, with minimal entropy generation at $\varphi = 1.5\%$ and $Re = 250$. Other studies, such as those by Yue *et al*. [15] and Sohankar *et al*. [16], highlight the role of surface wettability and slip flow in enhancing thermal and hydrodynamic performance.

The Lattice Boltzmann Method (LBM) [17-19] has emerged as a robust alternative to traditional Computational Fluid Dynamics (CFD) for simulating microscale [20]. Unlike CFD, LBM simplifies governing equations by solving the discrete Boltzmann equation, making it particularly suited for capturing microscale phenomena such as slip flow and rarefaction effects. It also offers high parallelizability, enabling faster computations on modern hardware like GPUs. Studies have demonstrated the efficacy of LBM in capturing complex phenomena, such as slip flow, temperature jump, viscous dissipation, and non-Newtonian fluid behavior, in microchannels [21]. For instance, Lalami *et al*. [22] investigated the role of Joule heating and viscous dissipation under MF conditions, revealing that superhydrophobic surfaces reduce viscous dissipation while enhancing HT. Similarly, Mehrizi *et al*. [23] examined the combined effects of MFs and nanoparticles on HT, reporting reduced friction with increased slip but highlighting the trade-offs with pressure drop under strong MFs. These studies underscore the importance of considering multifaceted interactions, yet they often address isolated phenomena rather than their combined effects. Afrouzi *et al*. [24] investigated the combined effects of nanoparticles, magnetic fields (MFs), and superhydrophobic surfaces on heat transfer (HT) and pressure drop in a microchannel. Their numerical simulations showed that while the inclusion of nanoparticles and MFs enhances HT, it also increases the pressure drop. In contrast, superhydrophobic surfaces were found to reduce pressure drop while maintaining a reasonable level of HT performance. Li *et al*. [25] analyzed the influence of surface hydrophobicity and MFs on HT in microchannels. Their simulations revealed that as surface hydrophobicity increases, HT decreases. However, MFs initially enhance HT, reaching a maximum at a Hartmann number (Ha) of 20. Beyond this value, further increases in the magnetic field strength result in a decline in HT performance. Geraeilinezhad *et al*. [26]examined the HT behavior of non-Newtonian pseudoplastic fluids in microchannels using the lattice Boltzmann method (LBM). This study specifically focused on the effects of slip boundary conditions and viscous dissipation. The results indicated that non-Newtonian fluids with a power-law index of 0.5 exhibit superior HT performance compared to Newtonian fluids. Nevertheless, the influence of viscous dissipation on HT was found to be minimal.

This study aims to expand the understanding of heat transfer improvement in microchannels by systematically investigating three synergistic mechanisms: non-Newtonian fluid behaviour, hydrophobic wall slip effects, and magnetohydrodynamic (MHD) phenomena. This study utilises the Lattice Boltzmann Method (LBM) to meticulously assess thermal and hydrodynamic performance under laminar flow conditions ($Re = 25$), focussing on the interplay between power-law rheology, velocity slip ($B = 0$-0.06), and transverse magnetic fields ($Ha = 0$-20). The analysis offers quantitative evaluations of heat transfer enhancement, viscous dissipation impacts, and pressure drop attributes, while determining ideal

operational conditions. These findings provide significant insights for the design of sophisticated thermal management systems in microelectronics and lab-on-a-chip applications, aiding the continuous advancement of efficient microscale heat transfer solutions that meet performance and energy efficiency criteria.

Numerical Methods

LBM is employed to simulate the non-Newtonian fluid flow and heat transfer (HT) characteristics in the microchannel. The LBM approach simplifies the complex Navier-Stokes equations by addressing the mesoscopic behavior of fluids through a distribution function (DF). This study utilizes the D2Q9 lattice model, which incorporates nine discrete velocity vectors for a 2D domain (Figure 1).

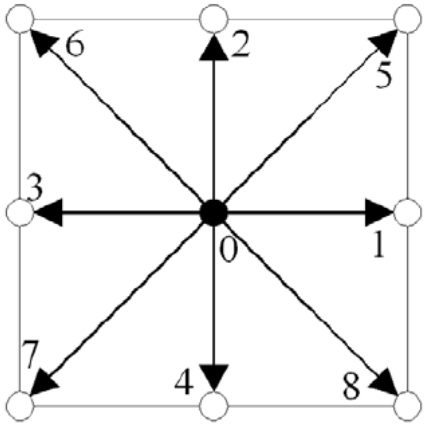


Fig. 1. D2Q9 lattice model for 2D physics

Instead of directly studying individual particles, the DF $f(\boldsymbol{r},\boldsymbol{c},t)$ is used to statistically describe the system. The DF evolves according to changes in molecule position and velocity:

$$\boldsymbol{r} \rightarrow \boldsymbol{r} + d\boldsymbol{r}, \quad \boldsymbol{c} \rightarrow \boldsymbol{c} + \boldsymbol{F}dt$$

where $\boldsymbol{F}$ represents the external force acting on the particles, and dt is the time step. The principle of conservation ensures that the number of molecules remains constant during motion and collisions.

The dynamics of the DF are governed by the Bhatnagar-Gross-Krook (BGK) form of the Lattice Boltzmann Equation [27]:

$$f_\alpha(\boldsymbol{x}+\boldsymbol{e}_\alpha\delta t, t+\delta t) = f_\alpha(\boldsymbol{x},t) - \frac{1}{\tau}[f_\alpha(\boldsymbol{x},t) - f_\alpha^{eq}(\boldsymbol{x},t)] + dtF_\alpha \quad (1)$$

where:

- $f_\alpha(\boldsymbol{x},t)$: DF in the discrete velocity direction α,
- $f_\alpha^{eq}(\boldsymbol{x},t)$: equilibrium DF,
- τ: relaxation time,
- α: lattice velocity direction.

The MHD source term in LBM can be calculated as:

$$F_\alpha = \frac{1}{\gamma^2} w_\alpha \left(1 - \frac{\Delta t}{2\tau}\right)\left[\frac{C_\alpha\cdot\vec{V}}{C_s^2}\left(\frac{C_\alpha\cdot\vec{V}}{C_s^4}\right)C_\alpha\right]\cdot\rho_0\vec{a} \quad (2)$$

where the acceleration due to the magnetic field, $\vec{a}$, can be calculated as:

$$\vec{a} = ax\vec{\imath} + ay\vec{\jmath} = -\frac{B_0^2\sigma_{nf}}{\rho}\vec{\imath} + 0\vec{\jmath} \quad (3)$$

where the following relation exists:

$$B_0{}^2\sigma_{nf} = \frac{Ha^2\mu_{nf}}{H^2} \quad (4)$$

where Ha is Hartmann number and σ is the electric current of the fluid.

The equilibrium distribution function f_α^{eq} for fluid flow is defined as:

$$f_\alpha^{eq} = \omega_\alpha\rho\left[1 + \frac{\boldsymbol{e}_\alpha\cdot\boldsymbol{u}}{c_s^2} + \frac{(\boldsymbol{e}_\alpha\cdot\boldsymbol{u})^2}{2c_s^4} - \frac{\boldsymbol{u}\cdot\boldsymbol{u}}{2c_s^2}\right], \quad (5)$$

where:

- ω_α: Weight corresponding to the lattice direction α,
- $\rho = \sum_\alpha f_\alpha$: Fluid density,
- $\boldsymbol{u} = \frac{\sum_\alpha f_\alpha \boldsymbol{e}_\alpha}{\rho}$: Velocity vector,
- $c_s = \frac{1}{\sqrt{3}}c$ Speed of sound in the lattice.

The pressure (p) and viscosity (ν) are expressed as:

$$p = \rho c_s^2, \nu = \frac{(\tau-0.5)c_s^2}{\delta t} \quad (6)$$

The temperature distribution function $(g_\alpha(\boldsymbol{x},t))$ follows a similar evolution as the DF:

$$g_\alpha(\boldsymbol{x}+\boldsymbol{e}_\alpha\delta t, t+\delta t) = g_\alpha(\boldsymbol{x},t) - \frac{1}{\tau_s}[g_\alpha(\boldsymbol{x},t) - g_\alpha^{eq}(\boldsymbol{x},t)], \quad (7)$$

where τ_s is the thermal relaxation time.

The equilibrium distribution function g_α^{eq} for temperature is expressed as:

$$g_\alpha^{eq} = \omega_\alpha T(\boldsymbol{x},t)\left[1 + \frac{3\,\boldsymbol{e}_\alpha\cdot\boldsymbol{u}}{2\,c^2}\right], \quad (8)$$

where:

$T(\boldsymbol{x},t) = \sum_\alpha g_\alpha(\boldsymbol{x},t)$: Macroscopic temperature at position $\boldsymbol{x}$ and time t,

The collision step is expressed as:

$$\widetilde{f_\alpha}(\boldsymbol{x},t+\delta t) = \widetilde{f_\alpha}(\boldsymbol{x},t) - \frac{1}{\tau}[f_\alpha(\boldsymbol{x},t) - f_\alpha^{eq}(\boldsymbol{x},t)], \quad (9)$$

$$\widetilde{g_\alpha}(\boldsymbol{x},t+\delta t) = \widetilde{g_\alpha}(\boldsymbol{x},t) - \frac{1}{\tau_s}[g_\alpha(\boldsymbol{x},t) - g_\alpha^{eq}(\boldsymbol{x},t)]. \quad (10)$$

The streaming step updates the DFs as:

$$f_\alpha(\boldsymbol{x}+\boldsymbol{e}_\alpha\delta t, t+\delta t) = \widetilde{f_\alpha}(\boldsymbol{x}, t+\delta t), \quad (11)$$

$$g_\alpha(\boldsymbol{x}+\boldsymbol{e}_\alpha\delta t, t+\delta t) = \widetilde{g_\alpha}(\boldsymbol{x}, t+\delta t). \quad (12)$$

The apparent viscosity (μ_{app}) for non-Newtonian fluids is defined as:

$$\mu_{\text{app}} = K\dot{\gamma}^{n-1}, \quad (13)$$

Where τ is Shear stress, $\dot{\gamma}$ is Shear rate, K is Consistency coefficient and n is flow behavior index.

This relationship indicates that the apparent viscosity depends on the shear rate and can exhibit the following behaviors:

1. Shear-Thinning ($n < 1$): The apparent viscosity decreases as the shear rate increases, characteristic of fluids like blood or paint.
2. Shear-Thickening ($n > 1$): The apparent viscosity increases as the shear rate increases, typical of fluids like cornstarch suspensions.

The Reynolds number (Re), Prandtl Number (Pr) [28], Nusselt Number (Nu) and Brinkman Number (Br) [22] for non-Newtonian fluids is defined as:

$$\text{Re} = \frac{\rho u^{2-n} {D_h}^n}{K}, \text{Pr} = \frac{C_p K\left(\frac{u}{D_h}\right)^{n-1}}{k_f}, \text{Nu} = \frac{hD_h}{k_f}, \text{Br} = \frac{\mu u^2}{k(T_w - T_{\text{ref}})}, \quad (14)$$

D_h represents the hydraulic diameter, defined as $D_h = 2HC$ [22], and h is the HTC.

$$h = \frac{-k\frac{\partial T}{\partial y}|y = H_c}{T_w - T_{ref}}, \quad (12)$$

Here, T_w and T_{ref} denote the wall temperature and the reference temperature, respectively, which is the same as the entering fluid temperature T_{in}.

In the present study, the inlet velocity is assumed to be uniform, and a no-gradient boundary condition is applied at the inlet. The microchannel wall is maintained at a constant temperature, and velocity slip as well as temperature jump are considered. The details of the boundary condition equations are presented in Appendix A.

The definitions of shear stress and friction coefficients are given as follows:

$$\tau_w = \mu\frac{\partial u}{\partial y}, \quad (15)$$

$$C_f = \frac{\tau_w}{0.5\rho u_{\text{in}}^2}, \quad (16)$$

The bulk temperature (T_b) is expressed as:

$$T_b = \frac{\int_A \rho u\, T dA}{\int_A \rho u\, dA}, \quad (17)$$

where A is the cross-sectional area of the microchannel.

A sudden rise in temperature occurs at the surface under slip conditions. Assuming the surface temperature as T_s, the dimensionless temperature (θ_j) of the flow is derived as:

$$\theta_j = \frac{T_s - T_{\text{in}}}{T_w - T_{\text{in}}}, \quad (18)$$

The temperature jump (ΔT) at the wall is given by:

$$T_s = T_w + \zeta^*\frac{\partial T}{\partial Y}, \quad (19)$$

where:

- T_s: Surface temperature,
- T_w: Wall temperature,
- ζ^*: Non-dimensional coefficient related to temperature jump,
- $\frac{\partial T}{\partial Y}$: Temperature gradient normal to the wall.

The term ζ^* is expressed as the coefficient of temperature jump (non-dimensional):

$$\zeta^* = \frac{\zeta}{HC} = \frac{B2\Gamma}{\text{Pr}(\Gamma+1)}, \quad (20)$$

where:

- B: Slip coefficient

The **slip coefficient** (often denoted as β or B) quantifies the degree of velocity slip at a hydrophobic surface. It is a critical parameter in microfluidic and nanofluidic systems where rarefaction effects or surface characteristics become significant due to the small length scales or hydrophobicity involved.

- $\Gamma = \frac{C_p}{C_v}$: Heat capacity ratio (equal to 1 in this study).

These equations characterize the influence of wall slip and temperature jump on the thermal behavior of non-Newtonian fluids in the microchannel.

Computational Domain and Boundary Conditions

The study examines the behavior of non-Newtonian fluids flowing through a $2D$ microchannel with isothermal surfaces. The fluid properties are assumed to remain constant and independent of temperature variations. The geometry of the microchannel is rectangular, and the fluid flow is modeled using the power-law model to capture the non-Newtonian characteristics. The flow is considered steady, incompressible, and fully developed. The schematic representation of the microchannel, including boundary conditions and flow parameters, is illustrated in Fig. 2. At the inlet of the microchannel, the fluid enters with a uniform velocity (U_{in}) and temperature (T_{in}), while the walls are maintained at a constant temperature (T_w). The Reynolds number (Re) for the simulations is fixed at 25, ensuring laminar flow conditions. The hydrodynamic height of the channel is denoted by HC, which represents the characteristic length for non-dimensionalizing the governing equations. To investigate the effects of surface slip and magnetic field interactions, the study incorporates

a range of non-dimensional slip coefficients ($B = 0, 0.02, 0.04, 0.06$) and Hartmann numbers ($Ha = 0, 5, 10, 15, 20$). The slip boundary condition accounts for the hydrophobic nature of the channel walls, while the magnetic field is applied perpendicular to the fluid flow direction to study its impact on velocity, heat transfer, and boundary layer behavior. The computational domain is designed to capture the interaction between these variables, including the effects of viscous dissipation and thermal jump, which are critical for understanding the heat transfer mechanisms in non-Newtonian fluids under such conditions. The outlet boundary condition ensures fully developed flow, allowing the investigation of the influence of inlet parameters and surface properties on the thermal and hydrodynamic performance of the microchannel.

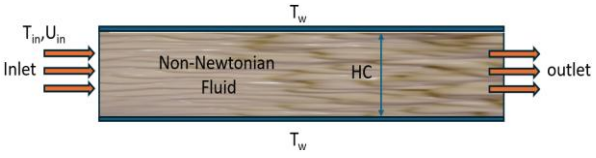


Fig. 2: Schematic Representation of the Microchannel Geometry and Boundary Conditions

Validation and Nesh Study

The velocity distribution in a specific cross-section of the microchannel was analyzed to verify the hydrodynamic behavior of the flow. Figure 3 presents a comparison of the velocity profiles obtained from the current study with the results reported by Rakotomalala [25] for different power-law indices (n). The results demonstrate a high level of agreement, confirming the reliability of the computational model. Specifically, the velocity profiles for n=1.0 (Newtonian fluid) and n=0.6 (non-Newtonian fluid) show close matching with the reference data.

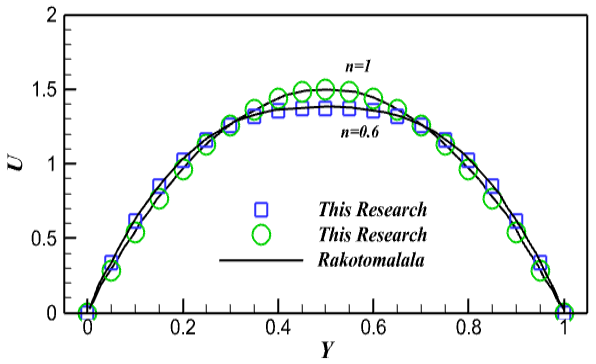


Fig. 3: Profile of non-dimensional velocity versus ref [29]

For extra validation, the Nusselt number is juxtaposed with the experimental findings of Manay and Sahin [30] across three distinct cross sections of a microchannel. This analysis is conducted within a microchannel measuring 200 μm in height and 50 mm in length, utilizing a nanofluid composed of 2% Titanium in water as the base fluid, which flows at a mass flow rate of 37.7 kg/h. The results of the comparison are displayed in table 1.

Table 1
validation of present study Nu number by comparison with reff [30] for water at mass flow rate of 37.7 kg/h.

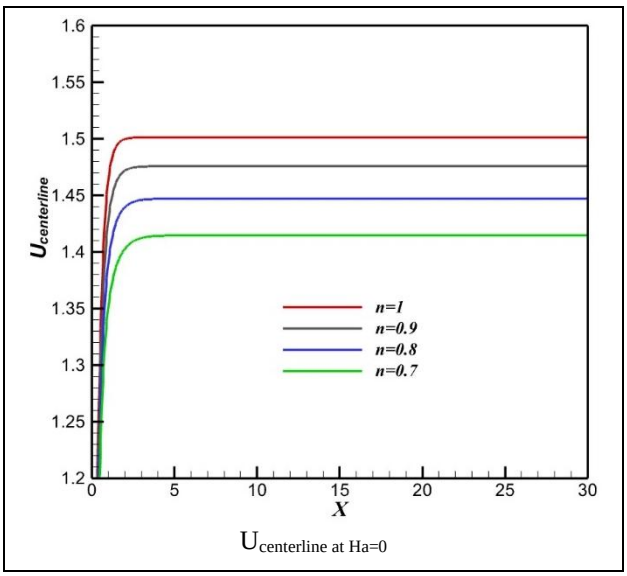
	x (m)	0.007	0.0275	0.0475
Pure water	Nu (present)	9.31	6.44	5.77
	Nu [30]	10.21	6.76	5.47
	error percentage	-8.77	-4.33	6.28

To ensure the reliability of the numerical results, a grid independence study was performed for Re = 25. Various grid sizes were tested, and the resulting values for the average Nusselt number (Nu_{ave}) and the friction coefficient (C_f) are presented in Table 2. The results indicate that as the grid resolution increases, the values of Nu_{ave} and C_f converge. A computational grid size of 30×900 was selected for the present investigation as it provides an optimal balance between accuracy and computational efficiency.

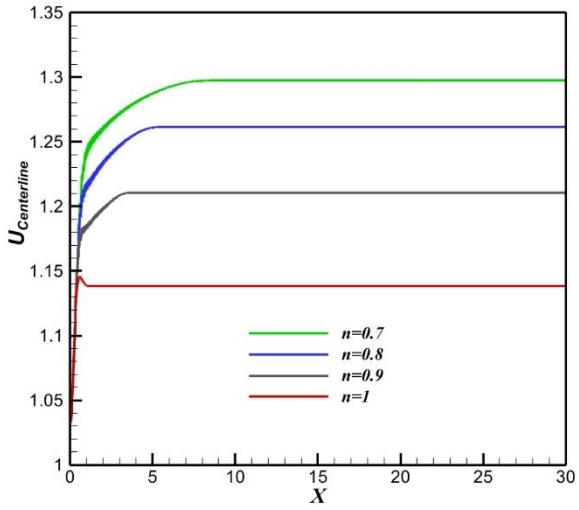
Table 2
Average Nuave and Cf for n=0.7 and B=0.02

Mesh	Nu_{ave}	C_f
20×600	3.95	0.104
24×720	4.07	0.119
30×900	4.11	0.123
36×1080	4.13	0.125

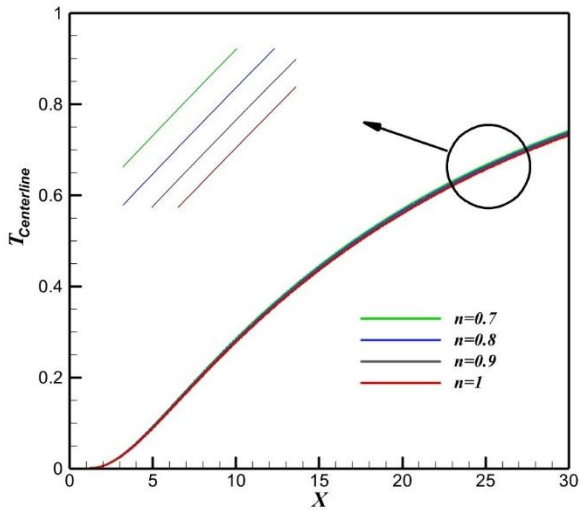
Figures 4 illustrates the variation of x-velocity and temperature values in the centerline of the channel under different MF strength (Ha=0,20) and different power law index (n=0.7, 0.8, 0.9 and 1). For observations Without Magnetic, as the power-law index (n) decreases, the boundary layer becomes thinner, and the central velocity of the fluid decreases. This behavior is attributed to the reduced resistance of the fluid to shear stresses at lower n values, which inhibits the growth of the boundary layer.



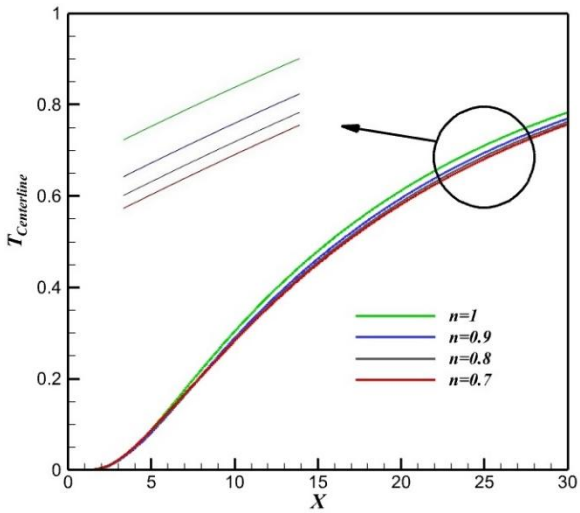
U centerline at Ha=0



$U_{centerline\ at\ Ha=20}$



$T_{centerline\ at\ Ha=0}$



$T_{centerline\ at\ Ha=20}$

Fig. 4. Local Temperature and velocity variation in the absence and presence of MF for various power-law indices.and two Ha of 0 and 20

Consequently, the thermal penetration from the channel wall to its core is more pronounced in the absence of an MF. For observations With Magnetic Field (Ha = 20), the presence of an MF modifies the flow dynamics significantly. The Lorentz force introduced by the MF interacts with the fluid's rheological properties, as quantified by the power-law index. An increase in Ha results in a thinner boundary layer and a reduction in axial velocity within the microchannel, which retards the thermal penetration into the channel core. Interestingly, under the influence of an MF, the trend reverses for the power-law index. A decrease in *n* leads to an increase in the central velocity and a thicker boundary layer, contrary to the zero-MF case. Figure 5 illustrates the relationship between the average Nusselt number (Nu_{ave}) and the slip length (B) under different magnetic field (MF) intensities, represented by Ha = 0 (non-magnetic case) and Ha = 15. Solid lines depict the results for Ha = 15, while dashed lines correspond to the non-magnetic case (Ha = 0). At Ha = 0, as the power-law index (n) increases from 0.7 to 1.0, the Nu_{ave} decreases due to changes in the velocity profile at the channel center and variations in the boundary layer thickness along the wall, leading to less efficient heat transfer. In contrast, at Ha = 15, this trend is reversed, and Nu_{ave} increases as n rises from 0.7 to 1.0. This behavior is attributed to the Lorentz force exerted by the MF, which modifies the fluid dynamics and enhances heat transfer within the microchannel. The introduction of slip length (B) has a notable impact on Nu_{ave}. Initially, at B = 0.02, Nu_{ave} decreases for both magnetic and non-magnetic cases. However, as B increases beyond B = 0.02, Nu_{ave} begins to rise again. This increase can be explained by the enhanced velocity difference between the fluid and the wall as B grows, which leads to changes in the boundary layer thickness and central velocity of the fluid. Consequently, the heat transfer efficiency improves with higher B. These findings highlight the complex interplay between the slip length, power-law index, and magnetic field intensity, demonstrating the importance of controlling B and Ha to optimize thermal performance in microchannels.

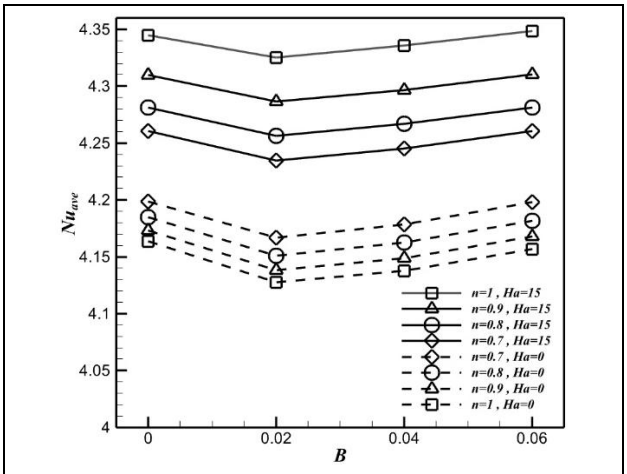


Fig. 5. Effect of MF on the variation of Nu_{ave} versus B

Figure 6 illustrates the variation of the average Nusselt number (Nu_{ave}) with the Hartmann number (Ha) for a power-law index of n=0.9. The results are presented for both the no-slip condition (B=0) and a slip condition with B=0.06. As shown, Nu_{ave} increases consistently with increasing Ha, reflecting the influence of the magnetic field on heat transfer enhancement. At intermediate Hartmann numbers (Ha = 5,10,15), there is no significant difference in Nu_{ave} between the no-slip and slip conditions. However, in the absence of a magnetic field (Ha = 0), the $Nu_{ave}$for the no-slip surface (B=0) is higher than that for the surface with slip (B=0.06). This behavior can be attributed to the weaker convective mechanism caused by slip at the wall. Conversely, at Ha = 20, the trend is reversed. The Nu_{ave} for the slip condition (B=0.06) surpasses that of the no-slip condition (B=0). This indicates that at higher magnetic field intensities, the slip condition contributes positively to heat transfer by altering the velocity profile and reducing the boundary layer thickness, thereby enhancing the convective heat transfer mechanism.

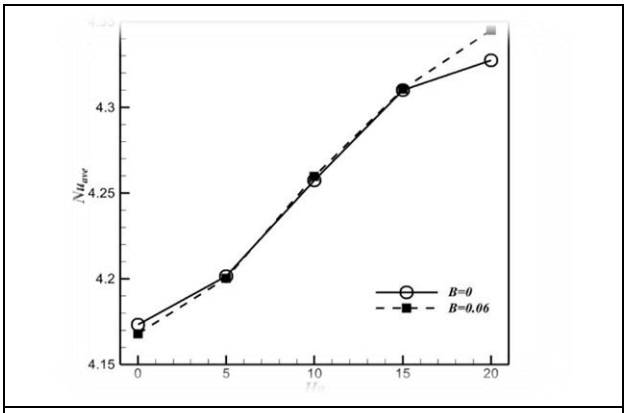


Fig. 6. Effect B on the variation of Nu_{ave} in the case of no viscous dissipation and temperature jump, and n=0.9

Figure 7 illustrates the variation of the average Nusselt number (Nu_{ave}) with the power-law index (n) in the absence of a magnetic field (Ha=0). The solid lines represent cases without viscous dissipation and temperature jump effects, while the dashed lines correspond to cases where both viscous dissipation and temperature jump are present. The results indicate that as the slip length (B) increases, the Nu_{ave} also increases, regardless of whether viscous dissipation and temperature jump are included. This behavior can be attributed to the enhancement of the convective heat transfer mechanism caused by the increased slip at the wall, which alters the velocity profile and improves heat transfer efficiency. Additionally, as the power-law index (n) increases, the Nu_{ave} decreases for all cases. This reduction is due to the thickening of the boundary layer and the diminished shear-thinning behavior at higher n values, which reduces the effectiveness of heat transfer. These findings highlight the interplay between slip length, power-law index, and the effects of viscous dissipation and temperature jump, emphasizing their significant roles in determining heat transfer performance.

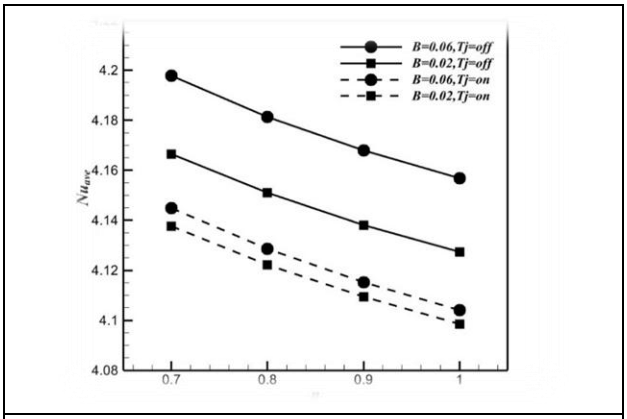


Fig. 7. Effects of viscous dissipation and temperature jump on the Nu_{ave} in the presence of a MF with Ha=0

Figure 8 illustrates the variation of the average Nusselt number (Nu_{ave}) with the power-law index (n) in the presence of a magnetic field (Ha=20). The solid lines represent cases without viscous dissipation and temperature jump effects, while the dashed lines correspond to cases where both effects are included. In the absence of viscous dissipation and temperature jump, increasing the slip length (B) results in an increase in Nu_{ave}. This enhancement is attributed to the increased convective heat transfer efficiency caused by the slip condition, which reduces the resistance to fluid motion near the wall, thereby promoting heat transfer. Conversely, when viscous dissipation and temperature jump are considered, increasing B leads to a decrease in Nu_{ave}. This reduction occurs because viscous dissipation generates additional heat within the fluid, altering the thermal boundary layer dynamics, while the temperature jump effects limits the thermal exchange between the wall and the fluid. Unlike the trend observed in the absence of a magnetic field (Figure 7), increasing the power-law index (n) in this case leads to an increase in Nu_{ave}. This behavior is due to the influence of the Lorentz force induced by the magnetic field, which modifies the velocity profile and enhances heat transfer as n increases. The results emphasize the complex interplay between slip, viscous dissipation, temperature jump, and the magnetic field in determining the thermal performance of non-Newtonian fluids in microchannels.

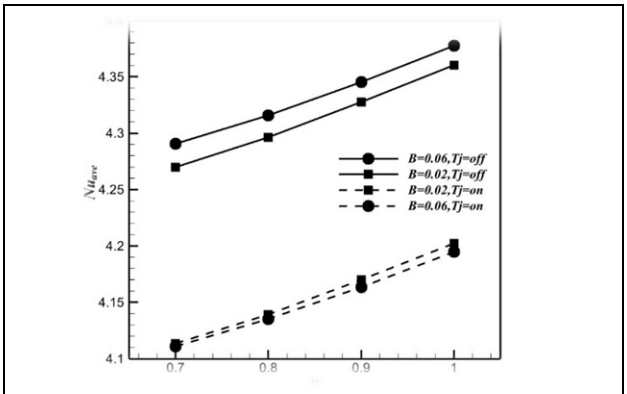


Fig. 8. Effects of viscous dissipation and temperature jump on the Nu_{ave} in the absence of a MF with Ha=20

Figure 9 shows the variation of the Nu_{ave} with the B. The effects of viscous dissipation and temperature jump are also presented for comparison. As the B increases, the slip velocity of the fluid at the surface increases, enhancing the convective HT mechanism. However, the inclusion of viscous dissipation and temperature jump results in a decrease in the Nu_{ave}, indicating a negative impact. Overall, increasing the slip velocity is beneficial, but the temperature jump effect counteracts this by reducing the HT potential. It is noteworthy that initially, as the B increases from B=0.02 to B=0.04 and beyond, the Nu_{ave} decreases, but eventually, the convective effect dominates and improves the HT mechanism.

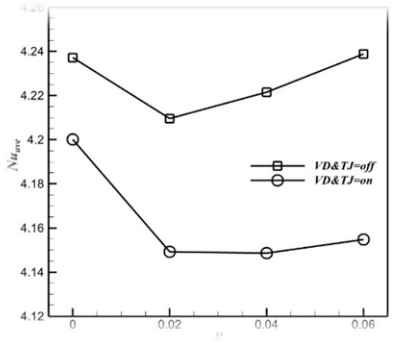


Fig. 9. Effects of viscous dissipation and temperature jump on the Nu_{ave} for various Bs at n=0.8 and Ha=10

Figure 10 shows the dimensionless temperature profile at the mid-section of the microchannel. The effect of the MF on temperature variations is considered (Ha=0, Ha=20). As observed, at the center of the microchannel for a Newtonian fluid (n=1) and a Ha of Ha=20, the fluid temperature is the highest, while in the absence of a MF (Ha=0), the fluid temperature is the lowest. The application of a MF reduces the fluid velocity at the center of the microchannel and alters the velocity profile across the section. The presence of the MF as an external force acting on the fluid flow leads to temperature changes at the center of the fluid and changes in the boundary layer growth. In the absence of a MF, decreasing the power-law index n also decreases the temperature, which is due to the reduced resistance of the fluid to shear stress. However, this behavior is reversed when a MF is present.

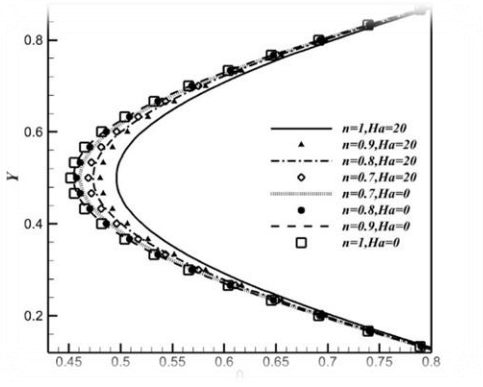
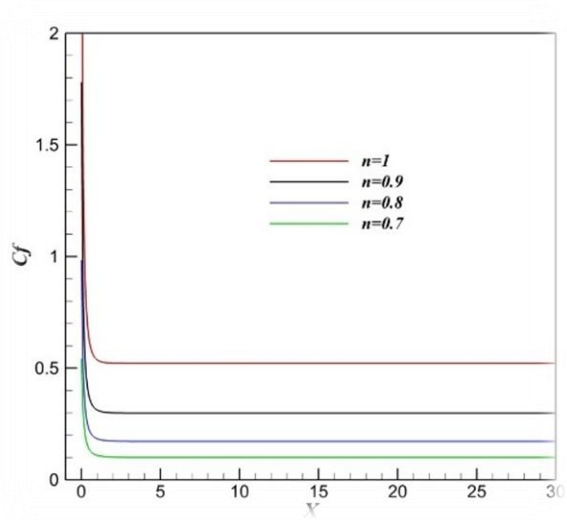
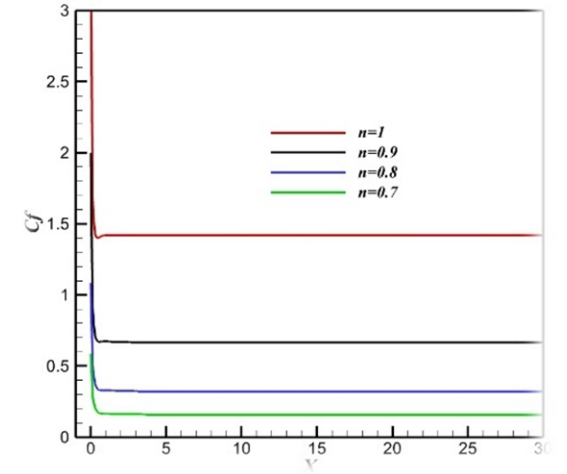


Fig. 10. Dimensionless temperature variation of the fluid in a microchannel cross-section for a B of B=0.06

Figure 11 presents the variation of the local friction factor along the length for different values of n. As can be seen, with decreasing n, the fluid behaves as a pseudoplastic fluid and exhibits less resistance to shear stress, resulting in a decrease in the local friction factor C_f. Additionally, Cf shows higher values for Ha=20 compared to Ha=0. This is due to the strengthening of the magnetic force and the consequent increase in shear stress between the surface and the fluid.



Ha=0



Ha=20

Fig. 11. Local friction factor along a microchannel for various power-law index *n*

Figure 12 displays the fluid velocity at the center of the microchannel along its length. As can be seen, in the case of no-slip and no MF (B=0, Ha=0), the maximum velocity occurs at the centerline of the microchannel. With increasing Ha and the introduction of slip at the surface, the centerline velocity gradually decreases, and according to the continuity principle, the velocity profile across the microchannel section changes. With the introduction of a B, the fluid slips at the surface, and with the formation of a new boundary layer, the velocity profile at the center of

the microchannel will also change. The MF, as an external term in the momentum equation, changes the net force acting on the fluid and plays a role in changing the fluid velocity.

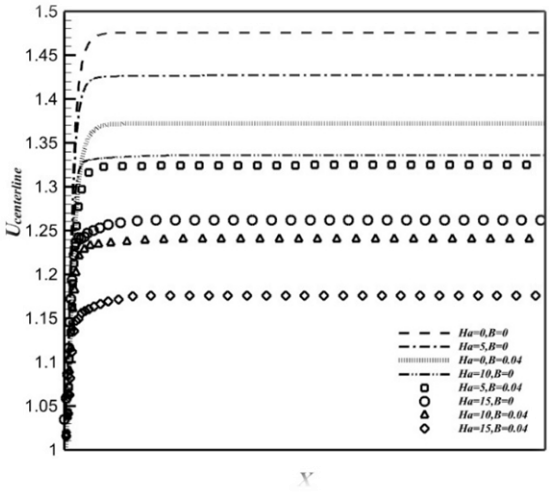


Fig. 12. Fluid velocity at the centerline along the microchannel

Figure 13 reveals the fluid velocity profile at the cross-section X=0.7 for n=0.7 and in the absence of a MF. As can be seen (elliptical), at the boundaries, due to the slip condition, the fluid velocity is no longer zero, and as the B increases, the slip velocity of the fluid on the surface increases, and the parabola opens wider, and the maximum value of the velocity profile decreases. In all these figures, the incompressibility of the fluid and the continuity equation are considered.

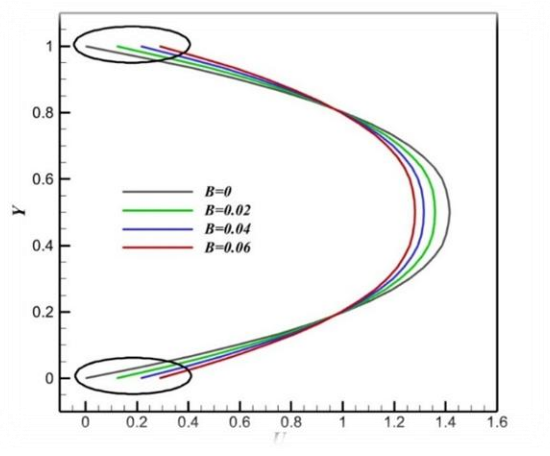


Fig. 13. Fluid velocity profile at cross-section X=0.7 for n=0.7, Ha=0

CONCLUSION

This study presents a comprehensive numerical investigation of heat transfer characteristics for non-Newtonian fluids in hydrophobic microchannels under the influence of magnetic fields. Using the Lattice Boltzmann Method (LBM), the effects of slip boundary conditions, viscous dissipation, and temperature jump were analyzed to understand their impact on thermal and hydrodynamic performance.

Key findings include:

- An increase in the power-law index leads to a decrease in fluid velocity and HT coefficient. This is attributed to the increase in apparent viscosity of the fluid with increasing power-law index.
- The application of a magnetic field results in a decrease in fluid velocity in middle section of channel and so a higher velocity gradient near channel surfaces.
- The higher magnetic field strength (Ha>15) starts enhancing heat transfer for higher slip coefficient (B=0.06) as it can make Nu number about 4% at this point.
- Increase in the nondimensional slip coefficient leads to an increment in fluid velocity near the wall. It decreases the HTP from B=0 to B=0.02 and after that it yields to enhance the HT rate.
- Neglecting viscous dissipation and temperature jump result in overestimating Nu number in the whole range of B.

These findings emphasize the complex interplay between slip conditions, non-Newtonian fluid rheology, magnetic field strength, and heat transfer mechanisms. They provide valuable insights for optimizing microchannel design in advanced cooling systems, particularly for applications in microelectronics and lab-on-chip devices.

REFERENCE

[1] Gao, J., et al., *Fluid flow and heat transfer in microchannel heat sinks: Modelling review and recent progress.* Thermal Science and Engineering Progress, 2022. **29**: p. 101203.

[2] Sadique, H. and Q. Murtaza, *Heat transfer augmentation in microchannel heat sink using secondary flows: A review.* International Journal of Heat and Mass Transfer, 2022. **194**: p. 123063.

[3] Song, G., et al., *Reviews: Applications of optimization algorithm for microchannel and microchannel heat sink on heat transfer.* International Journal of Heat and Fluid Flow, 2024. **108**: p. 109451.

[4] Fallah, K., et al., *Simulation of natural convection heat transfer using nanofluid in a concentric annulus.* Thermal Science, 2017. **21**(3): p. 1275-1286.

[5] Fallah, K., et al., *Numerical simulation of planar shear flow passing a rotating cylinder at low Reynolds numbers.* Acta Mechanica, 2012. **223**(2): p. 221-236.

[6] Eneren, P., Y.T. Aksoy, and M.R. Vetrano, *Experiments on single-phase nanofluid heat transfer mechanisms in microchannel heat sinks: A review.* Energies, 2022. **15**(7): p. 2525.

[7] Kumar, K., R. Kumar, and R.S. Bharj, *Entropy generation analysis due to heat transfer and nanofluid flow through microchannels: a review.* International Journal of Exergy, 2020. **31**(1): p. 49-86.

[8] Klazly, M. and G. Bognár, *A novel empirical equation for the effective viscosity of nanofluids based on*

theoretical and empirical results. International Communications in Heat and Mass Transfer, 2022. **135**: p. 106054.

[9] Nabwey, H.A., et al., *A comprehensive review of non-newtonian nanofluid heat transfer.* Symmetry, 2023. **15**(2): p. 362.

[10] Yıldız, G., Ü. Ağbulut, and A.E. Gürel, *A review of stability, thermophysical properties and impact of using nanofluids on the performance of refrigeration systems.* International journal of refrigeration, 2021. **129**: p. 342-364.

[11] Li, M., et al., *Experimental study on dynamic flow and heat transfer performance of silicon-based microchannel under variable thermal load.* International Journal of Heat and Fluid Flow, 2024. **110**: p. 109663.

[12] Qiu, Y., et al., *Experimental investigation of heat transfer and pressure drop in copper manifold microchannel heat sinks.* Applied Thermal Engineering, 2024. **255**: p. 124024.

[13] Rahbarshahlan, S., et al., *Numerical simulation of fluid flow and heat transfer in microchannels with patterns of hydrophobic/hydrophilic walls.* The European Physical Journal Plus, 2020. **135**(2): p. 157.

[14] Yao, Z., et al., *Numerical assessment of the impacts of non-Newtonian nanofluid and hydrophobic surfaces on conjugate heat transfer and irreversibility in a silicon microchannel heat-sink.* Journal of the Taiwan Institute of Chemical Engineers, 2023. **142**: p. 104642.

[15] Yue, C., et al., *Numerical study on flow and thermal characteristics of a micro-channel separated heat pipe under various surface wettability.* Case Studies in Thermal Engineering, 2021. **28**: p. 101345.

[16] Sohankar, A., M. Riahi, and E. Shirani, *Numerical investigation of heat transfer and pressure drop in a rotating U-shaped hydrophobic microchannel with slip flow and temperature jump boundary conditions.* Applied Thermal Engineering, 2017. **117**: p. 308-321.

[17] Fallah, K., et al. *Simulation of Planar Shear Flow Passing Two Equal-Sized Circular Cylinders in Tandem Arrangement*. in *AIP Conference Proceedings*. 2011. American Institute of Physics.

[18] Moafi Madani, S.M., et al., *Numerical study of geometric parameters effects on the suspended solid particles in the oil transmission pipelines.* Proceedings of the Institution of Mechanical Engineers, Part C: Journal of Mechanical Engineering Science, 2022. **236**(8): p. 3960-3973.

[19] Fallah, K., et al., *Numerical simulation of flow around two rotating circular cylinders in staggered arrangement by multi-relaxation-time lattice Boltzmann method at low Reynolds number.* World Applied Sciences Journal, 2011. **15**(4): p. 544-554.

[20] Fallah, K., et al., *Drop formation in cross-junction micro-channel, using lattice Boltzmann method.* Thermal Science, 2018. **22**(2): p. 909-919.

[21] Kalteh, M. and A. Alipour Lalami, *Investigation of the Effect of Velocity Slip and Temperature Jump on the Heat Transfer of Nanofluid in a Microchannel Under Constant Heat Flux with Lattice Boltzmann Method.* Amirkabir Journal of Mechanical Engineering, 2018. **50**(2): p. 255-270.

[22] Alipour Lalami, A. and M. Kalteh, *Lattice Boltzmann simulation of nanofluid conjugate heat transfer in a wide microchannel: effect of temperature jump, axial conduction and viscous dissipation.* Meccanica, 2019. **54**(1-2): p. 135-153.

[23] Mehrizi, A.A., et al., *Numerical investigation of conjugate heat transfer in a microchannel with a hydrophobic surface utilizing nanofluids under a magnetic field.* Physics of Fluids, 2021. **33**(5).

[24] Afrouzi, H.H., et al., *Thermo-hydraulic characteristics investigation of nanofluid heat transfer in a microchannel with super hydrophobic surfaces under non-uniform magnetic field using Incompressible Preconditioned Lattice Boltzmann Method (IPLBM).* Physica A: Statistical Mechanics and its Applications, 2020. **553**: p. 124669.

[25] Li, M., et al., *A comprehensive investigation of nanofluid conjugate heat transfer in a microchannel under MHD effect.* Alexandria Engineering Journal, 2023. **80**: p. 506-519.

[26] Geraeilinezhad, M., et al., *Numerical investigation of pseudoplastic fluid flow and heat transfer in a microchannel under velocity slip effect.* Engineering Analysis with Boundary Elements, 2023. **155**: p. 501-510.

[27] Mohamad, A., *Lattice boltzmann method*. Vol. 70. 2011: Springer.

[28] Sajadifar, S.A., A. Karimipour, and D. Toghraie, *Fluid flow and heat transfer of non-Newtonian nanofluid in a microtube considering slip velocity and temperature jump boundary conditions.* European Journal of Mechanics-B/Fluids, 2017. **61**: p. 25-32.

[29] Rakotomalala, N., D. Salin, and P. Watzky, *Simulations of viscous flows of complex fluids with a Bhatnagar, Gross, and Krook lattice gas.* Physics of Fluids, 1996. **8**(11): p. 3200-3202.

[30] Manay, E. and B. Sahin, *Heat transfer and pressure drop of nanofluids in a microchannel heat sink.* Heat Transfer Engineering, 2017. **38**(5): p. 510-522.

[31] Inamuro, T., M. Yoshino, and F. Ogino, *A non-slip boundary condition for lattice Boltzmann simulations.* Physics of fluids, 1995. **7**(12): p. 2928-2930.

[32] D'Orazio, A. and S. Succi. *Boundary conditions for thermal lattice Boltzmann simulations*. in *International Conference on Computational Science*. 2003. Springer.

Appendix A: Boundary conditions in lattice Boltzmann

1. Velocity

For velocity field at the channel inlet, a counter-slip method is used for incompressible preconditioned LBM with second order accuracy like as standard LBM [31, 32].

$$\rho_{in} = U_{in}\rho_0 + f_0 + f_2 + f_4 + 2(f_3 + f_6 + f_7) - \frac{\Delta t}{2}\rho_0 a_x U_{in} \quad (1)$$

$$\begin{aligned} f_1 &= \frac{w_1}{(w_1 + w_5 + w_8)}[\rho_{in} - (f_0 + f_2 + f_3 + f_4 + f_6 + f_7)] \\ f_{5\text{+}} &= \frac{w_5}{(w_1 + w_5 + w_8)}[\rho_{in} - (f_0 + f_2 + f_3 + f_4 + f_6 + f_7)] \\ f_8 &= \frac{w_8}{(w_1 + w_5 + w_8)}[\rho_{in} - (f_0 + f_2 + f_3 + f_4 + f_6 + f_7)] \end{aligned} \quad (2)$$

Second order extrapolation is applied at the channel outlet.

$$\begin{aligned} f_{3,m} &= 2f_{3,m-1} - f_{3,m-2} \\ f_{6,m} &= 2f_{6,m-1} - f_{6,m-2} \\ f_{7,m} &= 2f_{7,m-1} - f_{7,m-2} \end{aligned} \quad (3)$$

where m shows the last lattice node in horizontal direction and because of centerline symmetries:

$$\begin{aligned} f_4 &= f_2 \\ f_7 &= f_6 \\ f_8 &= f_5 \end{aligned} \quad (4)$$

2. Temperature

For temperature equation at the inlet like as velocity discretization, counter-slip approach is used to determine thermal boundary condition.

$$\begin{aligned} g_1 &= \frac{w_1}{(w_1 + w_5 + w_8)}[\theta_{in} - (g_0 + g_2 + g_3 + g_4 + g_6 + g_7)] \\ g_5 &= \frac{w_5}{(w_1 + w_5 + w_8)}[\theta_{in} - (g_0 + g_2 + g_3 + g_4 + g_6 + g_7)] \\ g_8 &= \frac{w_8}{(w_1 + w_5 + w_8)}[\theta_{in} - (g_0 + g_2 + g_3 + g_4 + g_6 + g_7)] \end{aligned} \quad (5)$$

For the channel outlet boundary condition, once again second order extrapolation is used as follows:

$$\begin{aligned} g_{3,m} &= 2g_{3,m-1} - g_{3,m-2} \\ g_{6,m} &= 2g_{6,m-1} - g_{6,m-2} \\ g_{7,m} &= 2g_{7,m-1} - g_{7,m-2} \end{aligned} \quad (6)$$

The real value of variables are obtained as following equations:

$$\begin{aligned} u(x,y)_{real} &= \left(\frac{u(X,Y)}{u_{in}}\right)_{Lattice} \times (u_{in})_{real} \\ v(x,y)_{real} &= \left(\frac{v(X,Y)}{u_{in}}\right)_{Lattice} \times (u_{in})_{real} \\ T(x,y) &= \theta(X,Y) \times (T_w - T_{in}) + T_{in} \end{aligned} \quad (7)$$

Where subscripts real and Lattice denote actual and Lattice Boltzmann scale respectively.

The velocity slip on the microchannel wall:

$$\vec{u}_s = \beta \frac{\partial \vec{u}}{\partial y} | y = 0 \quad (8)$$

In equation (7), $\vec{u}$ and β is the fluid horizontal velocity and slip coefficient respectively.

$$\overset{*}{U} = B \frac{\partial \overset{*}{U}}{\partial \overset{*}{Y}} \Big| \overset{*}{Y} = 0 \quad (9)$$

Here $\overset{*}{U}$ and B is the dimensionless velocity slip and slip coefficient respectively where:

$$B = {}^{\beta}/_{H_c} \quad (10)$$

We can use the second order forward derivative discretization[22]:

$$u_0 = \frac{B}{3B + 2\Delta \overset{*}{Y}}(4u_1 - u_2) \quad (11)$$

where u_0, u_1 and u_2 are horizontal velocity on the wall boundary and at first and second nodes above the lower wall respectively.